Journal of Intelligent & Robotic Systems (2019) 94:115–134
https://doi.org/10.1007/s10846-018-0956-8

Image Based High-Level Control System Design for Steering and Controlling of an Active Capsule Endoscope

Mehrnaz Aghanouri[1,2] · **Ali Ghaffari**[1] · **Nasim Dadashi Serej**[2]

Received: 12 February 2018 / Accepted: 7 November 2018 / Published online: 15 November 2018

Abstract

Using wireless capsule endoscopes for diagnosis and treatment of gastrointestinal tract disease has been increased in recent years. Due to the anatomical shape of the stomach, one of the most important challenges in capsule endoscopy is steering and controlling of the capsule inside the stomach to obtain the high-quality imaging. Another challenge is improving the accuracy of steering and controlling of the capsule, which is already highly dependent upon the operator's knowledge and skill who acts as a high-level controller. To address these challenges, in this paper, a novel image based High-Level Control system (H-LC) is proposed for real-time autonomous control of an active capsule endoscope. In the proposed system, first, a new desired path planning method based on detecting the stomach folds is implemented using the acquired images. Then, various maneuvers are presented for following the desired path and adjusting the orientation of the capsule. The core of these maneuvers is based on geometric analysis and computer vision techniques. The results for path planning method show the averages of Sensitivity 94%, Specificity 88% and Accuracy 92% on 82 endoscopic images of the stomach. For evaluating the proposed maneuver planning method, simulation in MATLAB is used. Based on the results, the suggested H-LC system can be used accurately for planning and following the desired path to achieve a more accurate control and steering of a capsule endoscope in a stomach with an unknown size.

Keywords Active capsule endoscope · Automatic endoscopy · Computer vision · High-level control · Path and maneuver planning

1 Introduction

The capsule endoscope is the new technology introduced in recent years for diagnosis and treatment of gastrointestinal tract (GI tract) disorders. One class of endoscopic capsules is the passive capsule endoscope, which is already widely used for examination of the small intestine [1, 2]. However, it may fail to acquire images from some important areas because its movement depends on peristaltic contractions. Another class of capsule endoscopes is active capsule endoscope whose movement is steerable and controllable. For this reason, this type of capsule endoscopes provides more reliable results [1, 3]. Active capsule endoscopes can help the clinician to take targeted biopsy and drug delivery. Besides, using this class of capsule endoscopes leads to decreasing the consuming energy, procedure time and the rate of capsule retention. Moreover, examination of the entire GI tract including the stomach can be possible by use of active capsule endoscopes [4]. Despite the many benefits, this class has not yet reached commercial production because there are various challenges related to it.

Achieving a complete autonomous capsule is one of the most important challenges [5]. In the literature, different methods, including lumen detection, vision-based and haptic

✉ Mehrnaz Aghanouri
maghanouri@mail.kntu.ac.ir

Ali Ghaffari
ghaffari@kntu.ac.ir

Nasim Dadashi Serej
nm.dadashi@gmail.com

[1] Faculty of Mechanical Engineering, K. N. Toosi University of Technology, Tehran, Iran

[2] Medical Image and Signal Processing Research Center (MISP), School of Advanced Technologies in Medicine, Isfahan University of Medical Sciences, Isfahan, Iran

feedback are proposed to assist in the steering and controlling of capsule endoscopes in GI tract [6, 7]. In [6], a method is suggested to partial automation of capsule navigation based on lumen detection in colon. Information achieved from lumen detection can help in capsule reorientation. In [7], a novel robotic visual and haptic based system for navigation of the capsule endoscope inside the colon is presented. In this system, the operator uses the haptic guidance module and 3D generated maps to navigate the capsule.

Another important challenge is steering and controlling of the active capsule endoscope inside the stomach due to the existence of large open space inside the stomach and its large anatomic size [8]. In this regard, different methods for autonomous steering and controlling of a capsule endoscope inside the stomach have been presented. Tortora et al. introduced a method for capsule endoscope's locomotion inside a liquid-distended stomach. In this method, the capsule exploits four propellers that their speeds and directions can be controlled by the user [9, 10]. Swain et al. presented a report in which a modified PillCam COLON capsule was used for housing a permanent magnet. This modified capsule was manipulated magnet in the human stomach by an external handheld permanent [11]. Rahman et al. used the Microcam-Navisystem to visualize the esophagus and stomach [12]. This system included a capsule containing a permanent magnet, a sensor belt that was fitted around the mid-torso of the patient, a receiver that was attached to the sensor belt, and an external handheld magnet. In another approach, Olympus Medical Systems Corp. and Siemens Healthcare developed a magnetically guided capsule endoscopy (MGCE) system, which consisted of the capsule endoscope with a small permanent magnet, the guidance magnet and the user interface [13, 14]. The capsule was steered inside the stomach by the physician using two joysticks. Carpi and his colleagues used a cardiovascular magnetic navigation system as an external robot for navigation of a magnetically modified endoscopic capsule inside the stomach [15, 16]. Mahoney and Abbott exploited a commercial 6-DOF robotic manipulator for 5-DOF manipulating of a magnetic capsule endoscope in fluid, which was similar to a fluid-distended stomach [17].

In all of the presented methods for steering and controlling of the active capsule endoscopes inside the stomach, the operator uses the acquired images by the capsule as the feedback for determining the new desired position and orientation of the capsule. In other words, the operator acts as a high-level controller. For example in [9, 10, 13–17] for steering and controlling of the capsule, first, the operator as a high-level controller specifies the desired values of the position and orientation of the capsule. Then, a low-level controller calculates the corresponding value of the actuator, and finally, the capsule is transferred to the new location. In [11, 12] the operator acts as both high-level and low-level controllers, i.e. by steering a handheld external magnet, he/she steers the capsule endoscope. It can be concluded that in all of the mentioned methods, the proper steering and controlling of the capsule inside the stomach depends on the operator's skills and experiences, which are difficult to achieve [1]. Since lack of operator's skills and his inaccuracies can lead to inappropriate imaging or non-imaging of some important areas, and ultimately lead to failure to detect disorders of the stomach, different researches have been done for enhancing the accuracy of imaging and facilitating the stomach diagnosis. These researches help the operator to steer and control of the capsule by adjusting its position and orientation using 3D surface reconstruction [7, 18, 19]. However, these methods are not very useful to address the mentioned problems above because the operator still acts as a high-level controller. In addition, 3D surface reconstruction using endoscopic images of the stomach is not accurate enough and has a high computational cost.

In this paper, a novel approach, a High-Level Control (H-LC) System is proposed. This system provides real-time automatic examination of the stomach (with an unknown size and exact shape) by autonomous control of an active endoscopic capsule equipped with only a monocular camera. In medical field, image-based control techniques are widely used generally for two purposes: 1. to assist the operator to determine the desired path, 2. to be used in the feedback of inner control loop (low-level controller) [20]. As it is stated in [20], the final state in visual servoing is fully automated surgery (image-based autonomous control), which is not still addressed in the existing literature. This approach is already used for image-based autonomous control of mobile robots in unknown environments. The main purpose of these methods is the road recognition and the desired path planning for navigation of the mobile robots. For the road recognition and its separation from its surroundings, different techniques such as, recognizing road edges [21], estimating the road as a geometrical shape [22], using the vanishing point of the road [23], using color and texture segmentation [24], using pixels classification [25], using image segmentation base on graph [26], and extracting the road contour using image segmentation and classification [27], have been presented.

In this paper, the proposed autonomous control method is achieved by planning the desired path and maneuvers based on the acquired images by the camera.

The core of the proposed H-LC system is detecting and following the folds of the greater curvature. First, a novel method is suggested for real-time planning the desired path using the acquired images as the feedbacks. Next, the desired path is followed using the proposed maneuvers. Then, a new method is proposed for maintaining

the direction of the capsule toward the wall of the stomach based on geometric modeling and analysis. Finally, the distance between the capsule and the wall is adjusted based on the method presented in our previous work [28]. This procedure leads to an automatic endoscopy while the capsule is steered autonomously from the fundus to the antrum. Using the suggested H-LC system, the desired positions and orientations of the capsule can be defined autonomously and without the need of an operator's intervention during the endoscopy procedure. Therefore, the accuracy of the stomach imaging and diagnosis is enhanced and an automatic endoscopy is provided.

The rest of this paper consists of 4 sections. In Section 2, the main purpose of this paper is explained more precisely and different phases of the high-level control system are presented. The simulation results and discussion are explained in Section 3, and finally in Section 4 the conclusion and future work are drawn.

2 Methods and Materials

The general system for automatic endoscopy by means of an active capsule endoscope inside the stomach is shown in Fig. 1. This system consists of three main parts: an active capsule endoscope, a high-level control system, which determines the desired path and maneuvers for autonomous control of the capsule, and a low-level controller for transmitting the proper commands to the actuators to reach the desired path and maneuvers. The main purpose of this paper is planning the desired path and maneuvers based on endoscopic images, called the high-level control (H-LC) system, for autonomous control of a capsule endoscope inside the stomach. This purpose is achieved in spite of the unknown exact shape and size of the stomach in different patients. The proposed control system provides a capsule endoscopy examination in which the capsule is not in contact (or is in minimum contact) with the walls of the stomach.

The stomach can be anatomically divided into several parts, including cardiac, fundus, body, lesser curvature, greater curvature, antrum and pylorus [29]. Each part has a special form and structural properties, which should be considered in designing the autonomous control system of the capsule. The presented H-LC system in this paper can be used specifically for imaging of the greater curvature, which is covered with the compact folds. The proposed high-level controller can be connected to every low-level controllers containing either internal locomotion or external locomotion. The locomotion mechanisms that are applicable to the free-floating capsule endoscopes are desirable. For this reason, magnetic levitation mechanisms (which are external locomotion) [30] and swimming mechanisms (which are internal locomotion) in a liquid-filled stomach cavity can be appropriate locomotion mechanisms.

The best position and orientation of the capsule during the automatic endoscopy will be achieved if 1. there is a distance between the capsule and the greater curvature, and 2. the optical axis of the capsule camera remains toward the greater curvature (Fig. 2). Since the capsule is not in contact with the greater curvature or any other walls, the stomach is exposed to less damage [31]. Besides, since the orientation of the capsule with respect to the greater curvature is similar to the conventional endoscopy by the flexible endoscope, it provides more accurate examination of the stomach [31].

The proposed H-LC system plans the desired path and the maneuvers regarding pre knowledge of the environment, initial position of the capsule, and three constraints: 1. the capsule should move on a path between the fundus and the antrum, 2. the capsule should do the imaging of the greater curvature while its camera's optical axis remains approximately perpendicular to the greater curvature during the movement, 3. the capsule should not have any contact with the walls of the stomach.

Before starting the use of H-LC system a primary step, including calibration and parking stages, is performed (Section 2.1). In H-LC system, autonomous control is done discretely and it consists of different movement steps. Each movement step comprises 4 phases: planning the desired path, following the desired path, maintaining the camera direction, and adjusting the distance (Sections 2.2 to 2.5) (Fig. 3).

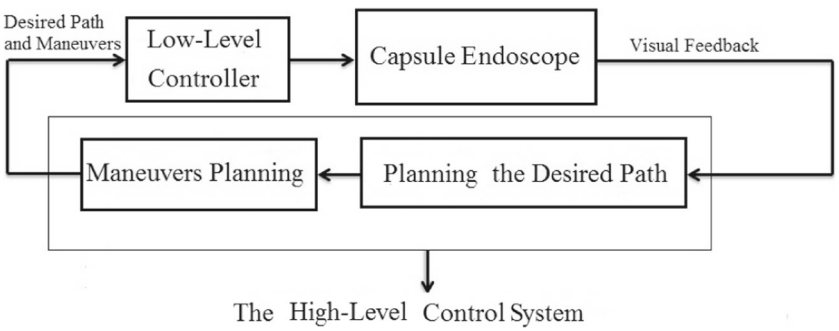

Fig. 1 The schematic of the general control system for automatic capsule endoscopy inside the stomach

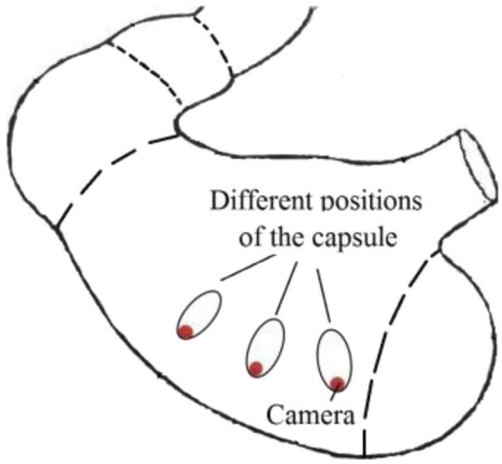

Fig. 2 The best position and orientation of a capsule endoscope with respect to the greater curvature when the patient lies on his left side

2.1 Primary Step

2.1.1 Calibration

The proposed calibration process is done in vitro using the capsule endoscope and a phantom model of stomach only one time for each type of the capsule endoscope. First, a line, whose length is equal to the desired translation value of the capsule along the greater curvature (Δx) in each movement step, should be drawn on the greater curvature of the phantom model (line AB in Fig. 4). Then, the camera (capsule) is manuaaly placed Z_0 cm far away from the greater curvature of the phantom model of the stomach where the quality and the scale of the acquired image is satisfactory to the physician. According to the physicians' experiences, the proper value for Z_0 is 3 or 4 cm. In this position, image 1 is acquired and then, the number of pixels equivalent to Δx cm of the greater curvature of the phantom model (the number of pixels on line AB) is stored (k). After that, the camera is shifted 1 cm away along the optical axis ($\Delta z = -1$), the new picture is acquired and the scale factor between this image and image 1 is obtained (S_{-1}) [28]. This process is repeated for $\Delta z = -2, -3, 1, 2$, and 3 (when the value of Z_0 is selected as 4 cm) (Fig. 4), and for each Δz, the related scale factors are determined (Table 1).

2.1.2 Parking

The proposed parking stage is defined as placing the capsule at the beginning of the greater curvature (where the fundus meets the greater curvature). To make it easier for the operator to achieve this, two steps, including initial parking and secondary parking are suggested. The reference coordinate system and the body coordinate system are defined in each step.

Initial Parking: Immediately after passing through the gastroesophageal junction (GEJ) and cardiac, the capsule must be placed so that the camera is directed toward the cardiac. In the other words, at the initial parking, the current image should display the cardiac. After parking the capsule, the initial reference coordinate system is defined as Fig. 5a. Here, the body coordinate system and the initial reference coordinate system are coincident.

Secondary Parking: The capsule is rotated about Y_{P1} in the positive direction while the fundus is displayed in the images. When the folds appear in the image from the middle to the last columns, the rotation stops and the rotation angle is stored. As a result, the direction of the capsule is perpendicular to the beginning part of the greater curvature. Then, the capsule is moved along the new Z-axis until a high quality image with the proper zoom and scale is acquired according to the operator's preference (since the selected quality and the scale of the image in this step and in "calibration" step are approximately the same, it can be concluded that the distance between the capsule and the greater curvature is approximately equal to Z_0). Now the new axes are defined as the second reference coordinate systems shown in Fig. 5b. In this step the body coordinate

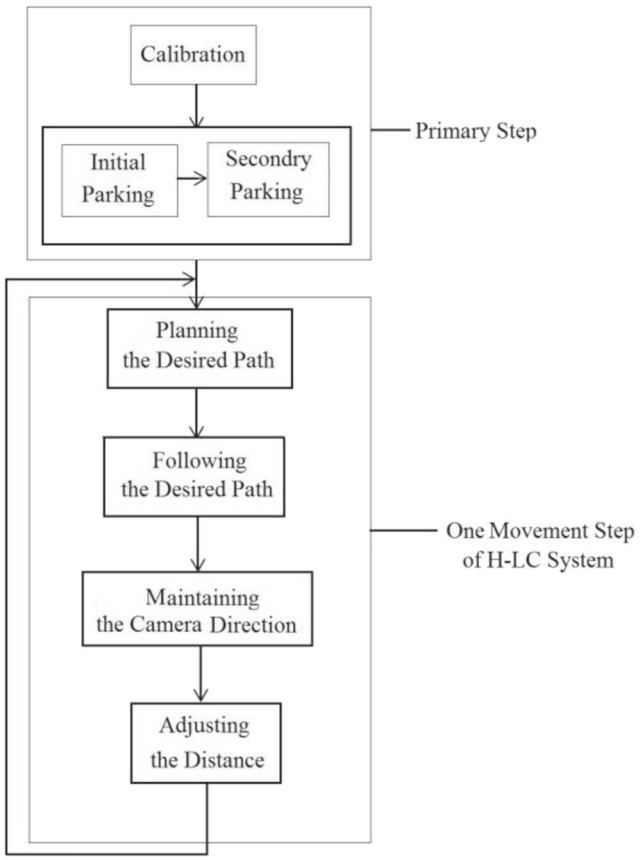

Fig. 3 The schematic diagram of the presented high-level control system

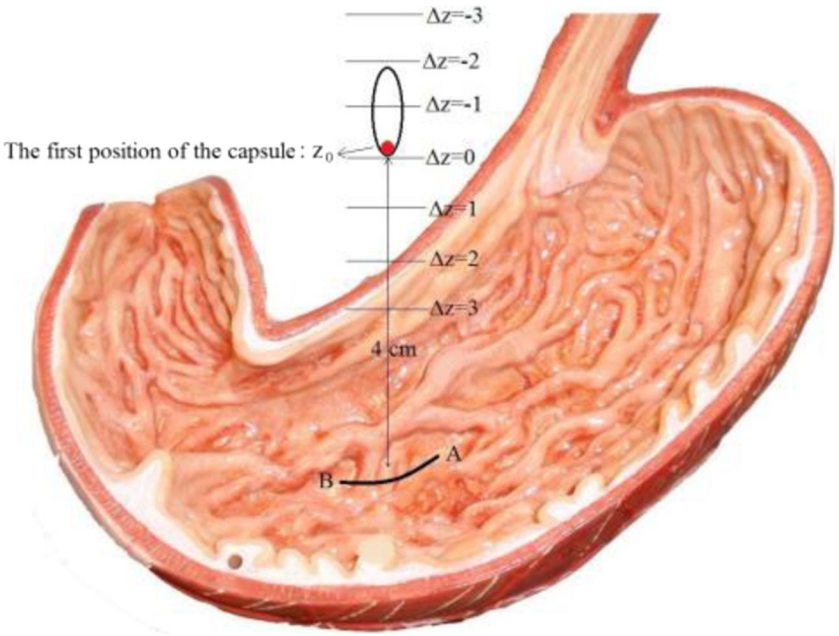

Fig. 4 The phantom model of the stomach, different positions of the capsule endoscope with respect to the greater curvature in calibration, and line AB

system and the second reference coordinate system are coincident. After the secondary parking, the capsule is ready for imaging of the greater curvature.

2.2 Planning the Desired Path

The main purpose in path planning is detecting the boundaries of the folds and defining the desired path in the middle of the region where the folds are restricted to in each frame. To this end, none of the methods mentioned above in Section 1, can be used for detecting the boundary of the folds because the region where the folds are restricted to in endoscopic images doesn't have any distinguishable edge, specific shape and structure, clear color variation, and uniform illumination.

Table 1 The data that are obtained in calibration

Capsule Displacement Related to Its First Position (Δz)	SCALE FACTORS (S)	Number of Pixels Equivalent to Δx cm of the Phantom's Greater Curvature
0	I	k
1	S_1	–
2	S_2	–
3	S_3	–
-1	S_{-1}	–
-2	S_{-2}	–
-3	S_{-3}	–

In this study, a new method is presented for detecting the boundary of the folds based on the endoscopic images of the greater curvature.

2.2.1 Detecting Folds Boundaries

For preparing the images to find the folds boundaries, first, the color image sent from the capsule to the computer is converted to grayscale. Then, two morphological operations, opening and closing [32], are applied to the image to make it smoother. Opening is an erosion followed by a dilation. The other operation, closing, is defined as a dilation followed by an erosion. The main goal of using morphological operations is smoothing the object's contours.

In order to detect folds boundaries, image segmentation based on geometric active contours is used. Active contours are deformable curves (or surfaces) used for finding object boundaries by moving within the images. Since in the endoscopic images the objects do not have specific edges and illumination is not uniform, in this paper, the region based model presented in [33] is used. This model is based on curve evolution techniques and level set method. After image segmentation and detecting the region where the folds are restricted to, the perimeter pixels, which demonstrate the boundaries, are extracted.

2.2.2 Defining the Desired Path

The desired path is planned based on the detected boundaries as follows:

Since the path of the folds is placed horizontally from left to right in the image, the desired path is also defined

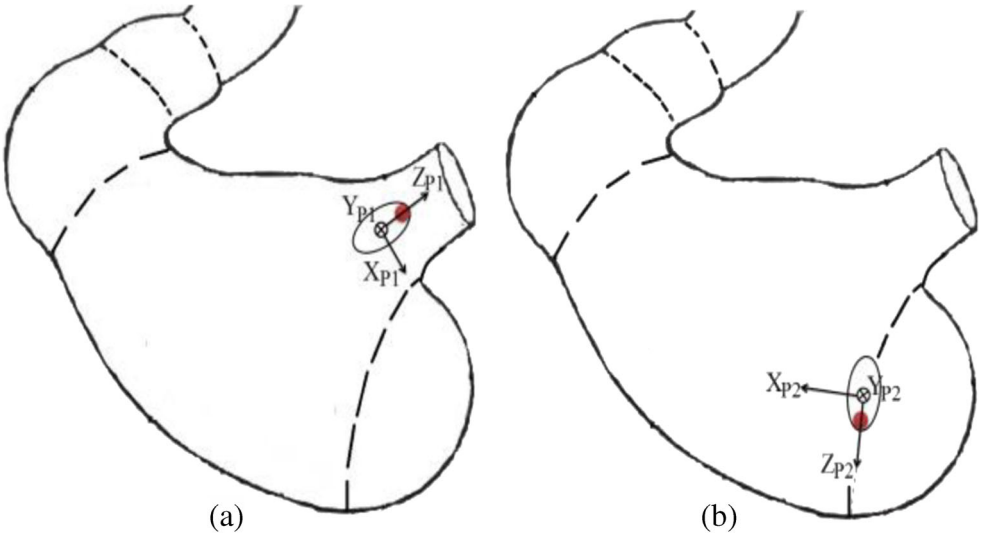

Fig. 5 The position of the capsule endoscope and the defined reference coordinate system after **a** initial parking, **b** secondary parking

horizontally. For planning the desired path, in each column of the image, the middle point between the pixel on the boundary closest to the first row and the pixel on the farthest boundary to the first row, are obtained. By using this method, the impact of the holes' boundaries, which are created because of the non-uniform illumination during the endoscopy, is removed. As a result, the desired path is located in the middle of the region where the folds are restricted to.

In some cases, the region where the folds are restricted to starts from the first or the last row of the image (Fig. 6). Since in these cases only one boundary is detected for the folds, in order to plan the desired path, the following steps should be done. Steps 1, 2, and 3 are defined for recognition of these cases. Step 4 is used for detecting another boundary for them, and in step 5 the desired path is planned.

1- The image that displays the perimeter pixels is considered. 10 columns of this image which are located at the distance of $j(=the number of the columns/10)$ from each other, starting from j/2th column, are selected. In each column, the quantity of the pixels whose intensity is equal to 1, is calculated and stored in i.
2- If the value of $i$is equal to 1 for at least 3 columns (it means there are 3 columns that the intensity of only one pixel in each of them is equal to 1), only one boundary has been found for the folds.
3- The numbers of the rows and the columns of the pixels mentioned in the previous step are stored.
4- The segmented image is selected. For each pixel whose coordinate is specified in step 3, the value of the intensity of the pixel at the row above it and at the same column is determined (I_r). If the value of I_r is equal to 0 for most of these pixels, it means that the folds are located in the region above the detected boundary because the region where the folds are restricted to is displayed in black. Therefore, the first row is assigned as another boundary. If the value of I_r is equal to 1 for most of them, it means that the folds are located in the region below the detected boundary consequently, the last row is assigned as another boundary.
5- In each column of the main image, the middle pixel between the pixel on the boundary which is determined in step 4, and the pixel on the farthest boundary to that, is selected. Finally the desired path, which is the path of folds, is planned.

In the cases that folds cover the whole of the image, no boundary is detected. If these cases occurred during secondary parking, no desired path is defined; otherwise the middle pixels between the pixels in the first and the last rows are selected as the desired path.

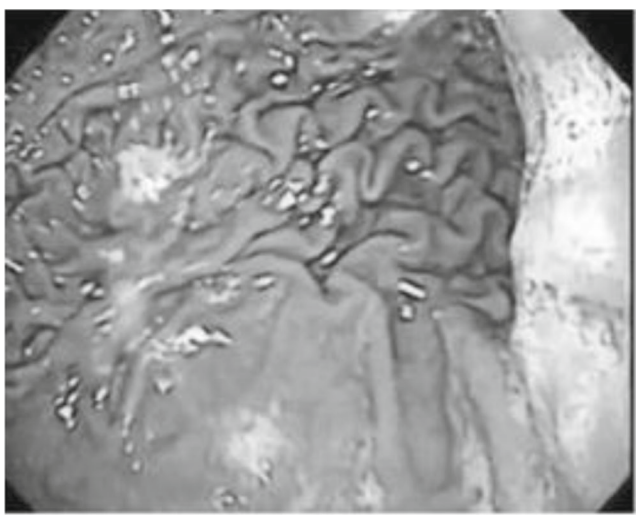

Fig. 6 An image of the greater curvature that the region where the folds are restricted to starts from the first row of the image

It should be noted that the pixels on the planned desired path and at the first and last columns of the image are not acceptable because there are four triangular black regions at the corners of the endoscopic images.

2.3 Following the Desired Path

For following the desired path, several maneuvers should be implemented.

First maneuver: to ensure that all of the folds inside the boundaries have been shown in the current frame, the desired path should be placed horizontally in the middle row of the image. To achieve this, first, the initial point of the desired path should be selected. This selection is based on the fact that the camera is against the greater curvature and its optical axis is considered approximately perpendicular to the surface of the greater curvature. Due to the camera's field of view, the points of the greater curvature that are placed exactly against the camera are appeared in the middle column of the acquired image (Fig. 7). Therefore the pixel on the desired path and in the middle column of the image is selected as the initial point (A).Then, a line (AB) is drawn between this point and the pixel on the desired path and in k columns ahead (B). Second, the angle between this line and the horizontal line (ψ) is calculated (Fig. 8). Finally, the capsule is rotated about the Z_{P2}-axis by ψ°. As a result, the part of the desired path (the path between two pixels) is located horizontally in the new image (Fig. 9).

Second maneuver: For transferring the horizontal line (AB) to the middle row of the image, first, the number of pixels between the initial point (A) and the pixel in the center of the image is measured and named m. Then, the capsule is translated along Y_{C1}-axis by Δy that is calculated as:

$$\Delta y = -\frac{m}{k^*} \tag{1}$$

Where k^* is the number of the pixels equivalent to the desired amount of the capsule's translation along the greater curvature in each movement step (Δx). Since the distance between the capsule and the greater curvature can be considered approximately constant and equal to Z_0 by applying phase 4 (Section 2.5), the value of k^*can be chosen equal to the value of $k$obtained in calibration.

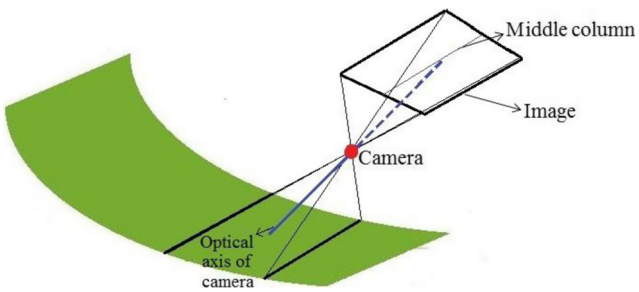

Fig. 7 The position of the camera which can be considered against the middle column of the acquired image when it is perpendicular to the scene

Third maneuver: for following the desired path, the capsule is moved Δx cm in the direction of X_{C2}-axis in each movement step. If the value of Δx is selected too large, enough matching interest points, which are necessary for adjusting the distance between the capsule and the greater curvature [28], are not detected. Therefore, the best value of $\Delta x$is 1 cm.

Figure 10 shows different maneuvers defined in this section.

2.4 Maintaining the Camera Direction

For maintaining the camera directed toward the greater curvature and approximately perpendicular to it, a rotation maneuver is introduced. In the proposed maneuver the capsule is rotated about Y_{C3}-axis by α°. The proposed method of determining α is based on geometric analysis. In order to show the position of the capsule with respect to the greater curvature, the surface of the greater curvature is projected on a cylindrical surface as shown in Fig. 11. R_{1_1} is the position of the capsule after the secondary parking and R_{2_1} is the position of the capsule after applying the introduced maneuvers in Section 2.2. For displaying the rotation of the capsule, the projection of the cylindrical surface on XZ-plane is used (Fig. 12).

After applying the introduced maneuvers in Section 2.2, the capsule at its new position is not perpendicular to the curve at point B. The rotation maneuver is applied so that the capsule becomes approximately perpendicular to the curve at point B'. The error of non-perpendicularity of the camera to the curve at point B' (E_1) can be obtained as:

$$E_1 = |\alpha - (\beta + \gamma)| \tag{2}$$

where β is the angle between the perpendicular line to the curve at point B (OB) and the horizontal line (OA), and γ is the angle between OB and OB'.

As it is shown in Fig. 12, the angle β can be assumed as:

$$\beta = \sin^{-1}\left(\frac{\Delta x}{R_a}\right) \tag{3}$$

where R_a is the radius of the cylindrical surface (greater curvature). Since R_a can be assumed larger than 2 cm in adult stomach and $\Delta x = 1$ (as it is mentioned in Section 2.3), β can be assumed a small angle and it can be approximated as:

$$\beta \approx \frac{1}{R_a} \tag{4}$$

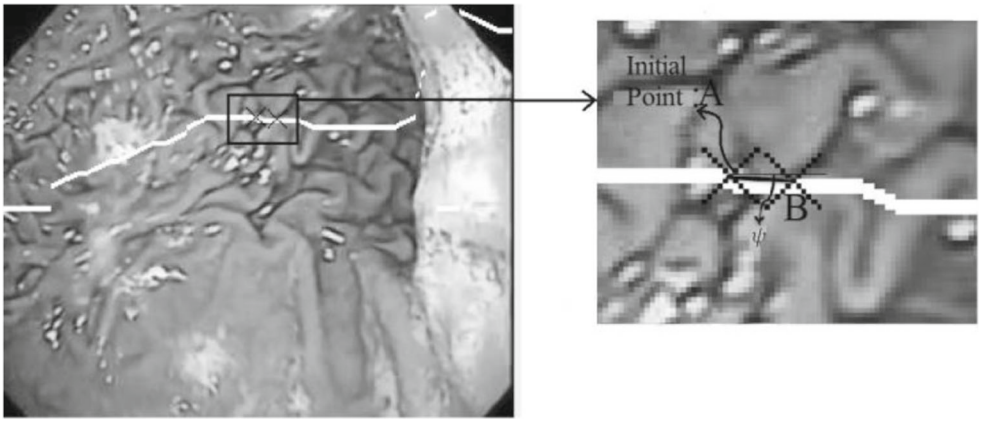

Fig. 8 Line AB and angle ψ on the desired path

In order to calculate γ in terms of α, Fig. 13 is considered and the length of $\overline{BB'}$ is calculated.

In triangle $BB''B'$:

$$\begin{cases} \widehat{BB'B''} = \beta + \gamma + \frac{180-\gamma}{2} - \alpha \\ \widehat{BB''B'} = 180 - \frac{180-(\alpha-\beta)}{2} \end{cases} \Rightarrow \widehat{B''BB'} = \frac{\alpha-(\beta+\gamma)}{2} = \frac{1}{2}E_1 \tag{5}$$

It can be concluded from Eq. 5 that for small error:

$$\overline{BB'} \cong \overline{BB''} \tag{6}$$

In triangle BOA':

$$\begin{cases} \overline{CB} = b - (R_a - R_a\cos(\beta)) \xrightarrow{for\ small\ \beta:\cos(\beta)=1} \overline{CB} = b \\ \overline{BO'} = \frac{h}{\sin(\alpha-\beta)} \xrightarrow{h=\overline{CB}\sin(\alpha)} \overline{O'B} = \frac{b\sin(\alpha)}{\sin(\alpha-\beta)} \\ \overline{OA'}||\overline{O'B''} \xrightarrow{Intercept\ theorem} \frac{\overline{BB''}}{\overline{BA'}} = \frac{\overline{BO'}}{\overline{BO}} \\ \Rightarrow \overline{BB''} = \overline{BA'}\frac{b\sin(\alpha)}{R_a\sin(\alpha-\beta)} \end{cases} \tag{7}$$

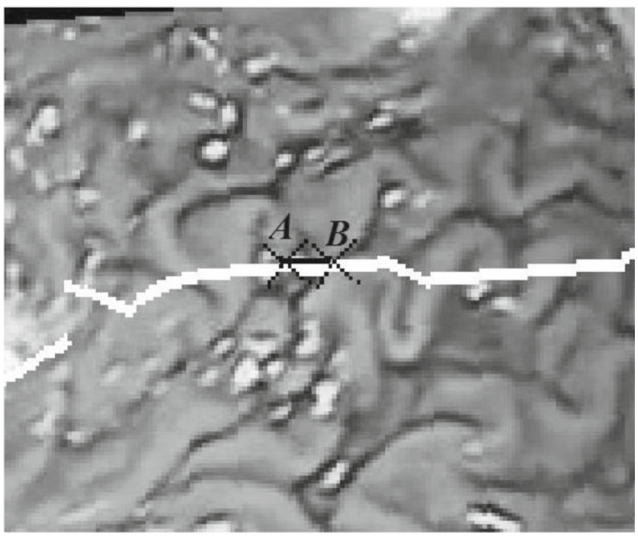

Fig. 9 The rotated image about Z_{P2} by ψ

where b is the distance between the center of capsule and the curve of the greater curvature. From Eqs. 6 and 7:

$$\overline{BB'} = \overline{BA'}\frac{b\sin(\alpha)}{R_a\sin?(\alpha-\beta)} \tag{8}$$

Now γ is calculated by using the relationship between chord and angle:

$$\begin{cases} \overline{BB'} = 2R_a\sin\left(\frac{\gamma}{2}\right) \\ from\ (8): \overline{BB'} = \overline{BA'}\frac{b\sin(\alpha)}{R_a sin(\alpha-\beta)} \\ \overline{BA'} = 2R_a\sin\left(\frac{\alpha-\beta}{2}\right) \end{cases} \Rightarrow \gamma = 2\sin^{-1}\left(2R_a\sin\left(\frac{\alpha-\beta}{2}\right)\frac{b\sin(\alpha)}{2R_a^2\sin(\alpha-\beta)}\right) \tag{9}$$

By supposing small α and β, Eq. 9 can be written as:

$$\gamma = \frac{b}{R_a}\alpha \tag{10}$$

By substituting Eqs. 4 and 10 in Eq. 2 the error of non-perpendicularity of the camera to the curve at point B'can be written as:

$$E_1 = \left|\alpha - (\frac{1}{R_a} + \frac{b}{R_a}\alpha)\right| = \frac{1}{R_a}\left|(R_a - b)\,\alpha - 1\right| \tag{11}$$

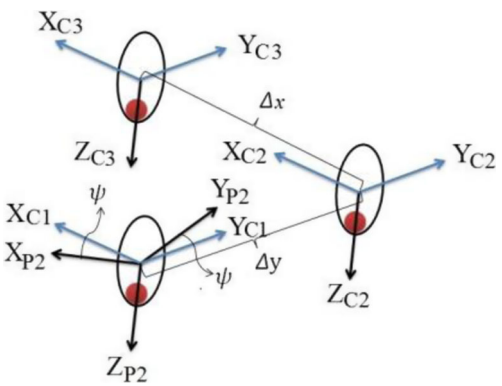

Fig. 10 The defined maneuvers for following the desired path

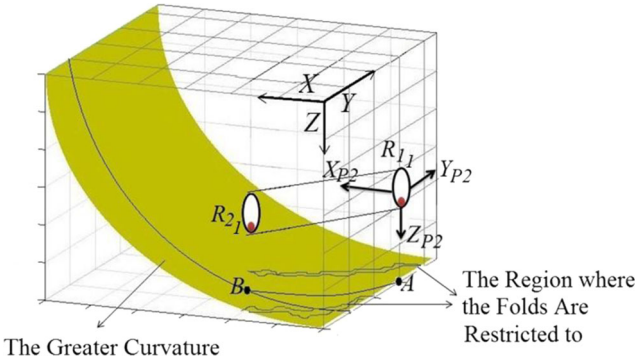

Fig. 11 The projection of the greater curvature on a cylindrical surface, and the positions of the capsule

For n_sth movement step the error is calculated as:

$$E_{n_s} = n_s \left| \alpha - \left(\frac{1}{R_a} + \frac{b}{R_a}\alpha \right) \right| = \frac{n_s}{R_a} \left| (R_a - b)\,\alpha - 1 \right| \quad (12)$$

The number of movement steps (N) is derived in Eq. 13 in terms of the length of the greater curvature (L in Fig. 12) and the length of arc AB'.

$$\begin{cases} N = \frac{L}{AB'} \\ AB' = a\,(\beta + \gamma) = R_a \left(\frac{1}{R_a} + \frac{b}{R_a}\alpha \right) = 1 + b\alpha \\ L = R_a \phi \end{cases}$$

$$\Rightarrow N = \frac{R_a \phi}{1 + b\alpha} \quad (13)$$

where ϕ is the central angle subtended by the greater curvature.

It can be understood from Eq. 12 that the error occurring at each step accumulates and becomes larger as the capsule travels along the greater curvature. The maximum error (E_N) happens at the last point of the greater curvature. For small α and β, the value of this error is:

$$E_N = \phi - N\alpha N = \frac{R_a \phi}{1 + b\alpha} \Rightarrow E_N = \phi \left(1 - \frac{R_a}{1 + b\alpha}\alpha\right) \quad (14)$$

The main purpose is finding the proper value of α which minimizes the error in each movement step. According to Eq. 12:

$$E_{n_s} = 0 \Rightarrow \alpha = \frac{1}{R_a - b} \quad (15)$$

Since the value of R_a varies for different patients, in order to calculate the proper α, a range should be defined for R_a. In different works e.g. [34] the shape of the distended stomach is estimated like a sphere, R_a can be considered as 6 cm for 1 liter distended stomach. On the other hand, the length of the greater curvature is 4 or 5 times longer than

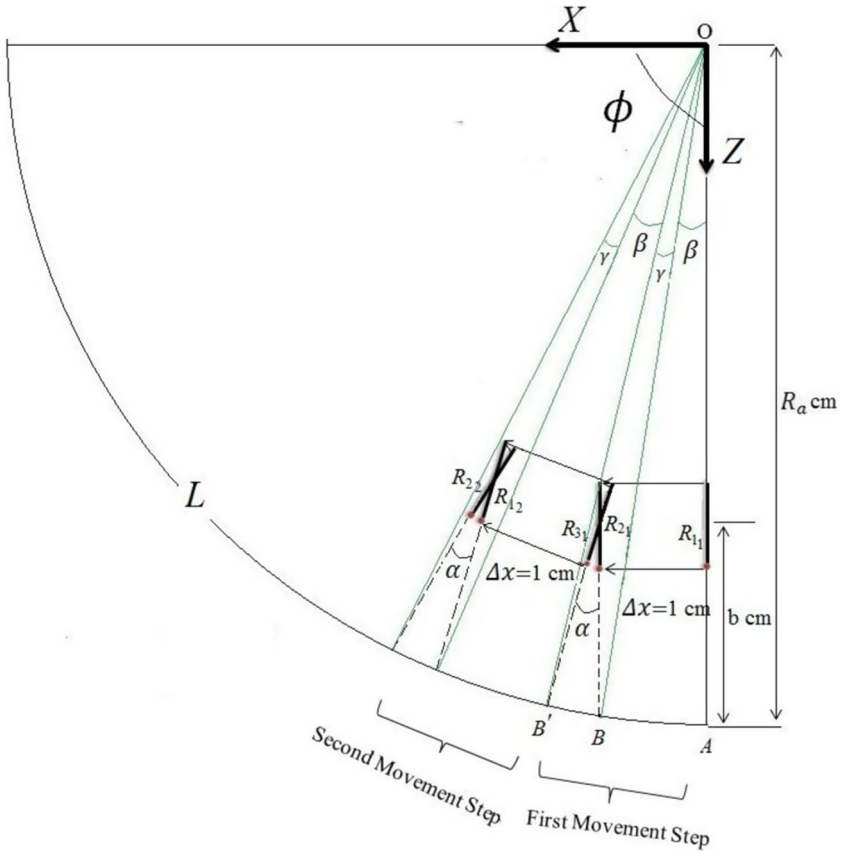

Fig. 12 The projection of the cylindrical surface in XZ-plane. R_3 is the position of the capsule after the rotation maneuver

the lesser [35] and according to [36], assuming the spherical geometry for the stomach is not valid. Hence, in order to achieve a more reliable value for R_a, three real stomachs were measured in dissection room of Isfahan University of Medical Science, and the largest value of $R_a$was obtained as 18 cm.

In order to determine the value of b, it is assumed that the length of the capsule endoscope is 2 cm and the proper distance between the camera and the greater curvature is 4 cm. As a result, the value of b can be determined as 5 cm.

Now, the proper range of α for zero error is calculated as:

$$6 \leq R_a \leq 20, b = 5$$

$$\Rightarrow 0.07rad \simeq 4^\circ \leq \alpha \leq 1rad \simeq 57^\circ \quad (16)$$

As it is mentioned before, the value of $R_a$varies for different people, so the proper value of α is also unknown. Therefore, the value of α is selected as 0.125 rad at first, which is corresponding to the median value of R_a(13 cm) and zero error. Then, the maximum error for different values of R_a is obtained. According to Eqs. 12 and 14, the maximum error occurs for $R_a = 6and20$ and for the last movement step, so the impacts of the non-perpendicularity error are investigated for these cases. These impacts are shown by three variables. The first and second variables indicate the common area between two images (CA_n) acquired by the camera at positions R_{1_n} (when the nth movement step starts) and R_{3_n} (after applying following the desired path maneuvers and rotation maneuver). This common area is corresponding to the common length of the greater curvature in XZ-plane seen in R_{1_n} and R_{3_n} positions. CA_n should be large enough to ensure there are sufficient corresponding interest points to be matched in two images [28]. CA_n decreases as the non-perpendicularity error increases, so its minimum CA_N occurs in Nth movement step. Therefore, the variables used for indicating CA_n are the length of the greater curvature which is seen by the camera in the last movement step (the arc NF) and the angle (ν) subtended by this arc (Figs. 14 and 15). The value of CA_N can be assumed as the value of NF.

The third variable (e_d) demonstrates the distance between the position of the camera at N-1th movement step and the part of the greater curvature which is displayed in the middle column of the acquired image in this movement step (Fig. 16). As it is mentioned in Section 2.3, for following the desired path, the pixel in the middle column of the image, which is located against the camera, is used. This distance is made because the position of the camera is not exactly against the middle column of the image when its optical axis is not perpendicular to the scene.

According to the general shape of the stomach and the measurements of ϕ, which are obtained from cadavers, the value of ϕ can be considered between 80 to 110 degrees.

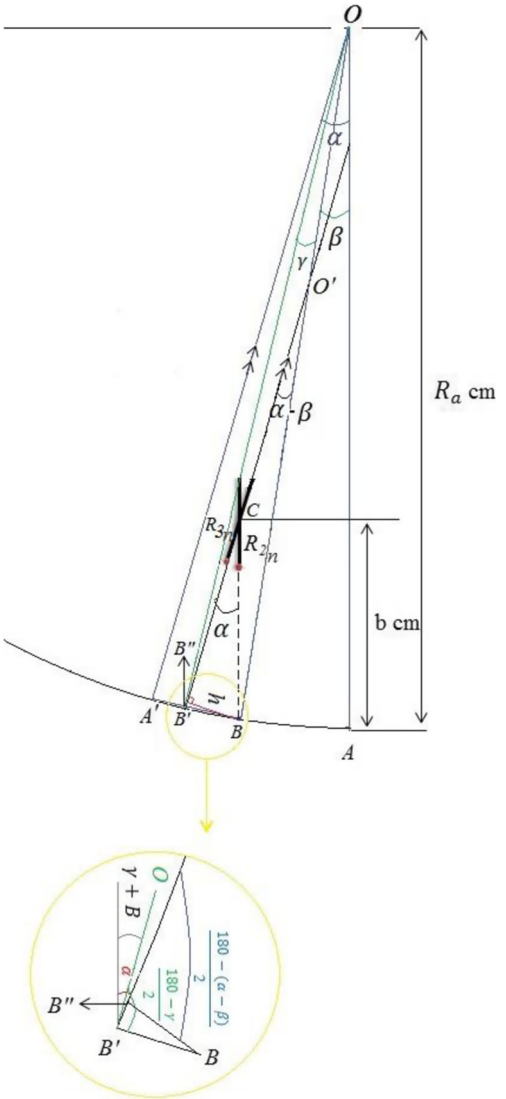

Fig. 13 The geometric information of the capsule movement along the greater curvature

The impacts of the non- perpendicularity error in the last movement step are investigated based on Fig. 14. By assuming the angle of view equal to 120° and the angular error greater than zero ($E_N > 0$):

$$\begin{aligned} x_{cam} &= R_a \sin(\phi) - 4\cos\left(\frac{\pi}{2} - \phi + E_N\right) \\ z_{cam} &= R_a \cos(\phi) - 4\sin\left(\frac{\pi}{2} - \phi + E_N\right) \end{aligned} \quad (17)$$

$$\begin{cases} x_{cam} + f\cos\left(\frac{\pi}{2} - \phi + E_N + \frac{\pi}{3}\right) = R_a \sin(\sigma) \\ z_{cam} + f\sin\left(\frac{\pi}{2} - \phi + E_N + \frac{\pi}{3}\right) = R_a \cos(\sigma) \end{cases}$$

$$\xrightarrow{\text{Raise both sided to the power of 2}} \left(x_{cam} + f\cos\left(\frac{\pi}{2} - \phi + E_N + \frac{\pi}{3}\right)\right)^2 + \left(z_{cam} + f\sin\left(\frac{\pi}{2} - \phi + E_N + \frac{\pi}{3}\right)\right)^2 = R_a^2 \quad (18)$$

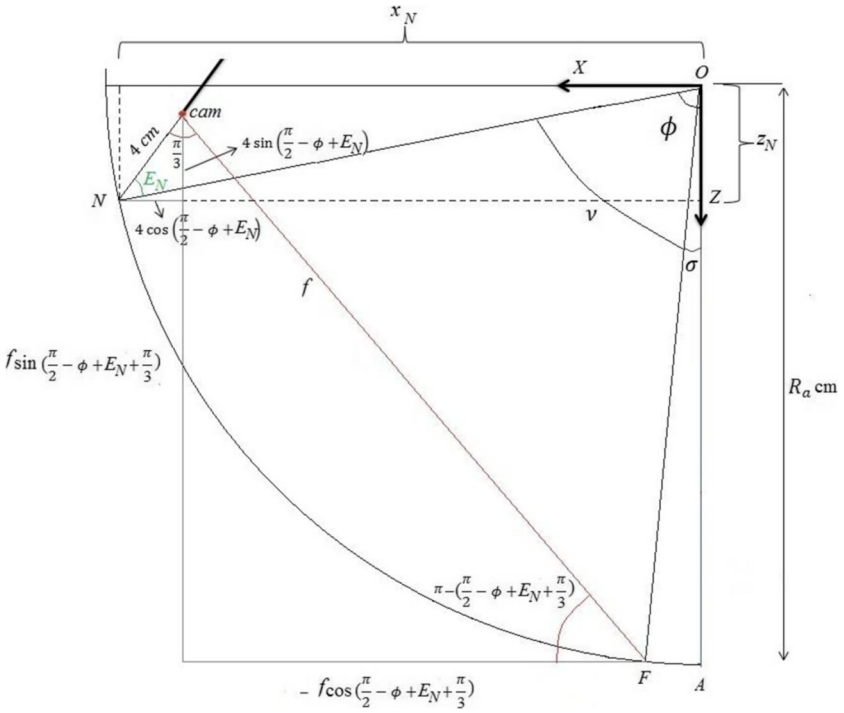

Fig. 14 The position of the capsule with respect to the greater curvature in *N-1*th movement step for $E_N > 0$

f can be calculated using Eq. 18. Accordingly, the coordinates of point $F$is obtained as:

$$\begin{aligned} x_F &= x_{cam} + f\cos\left(\frac{\pi}{2} - \phi + E_N + \frac{\pi}{3}\right) \\ z_F &= z_{cam} + f\sin\left(\frac{\pi}{2} - \phi + E_N + \frac{\pi}{3}\right) \end{aligned} \tag{19}$$

Finally, the length of the greater curvature, which is seen by the camera in the last movement step (the arc *NF*), and the angle (ν) subtended by this arc are derived as:

$$\nu = \phi - \tan^{-1}\left(\left|\frac{x_F}{z_F}\right|\right)$$

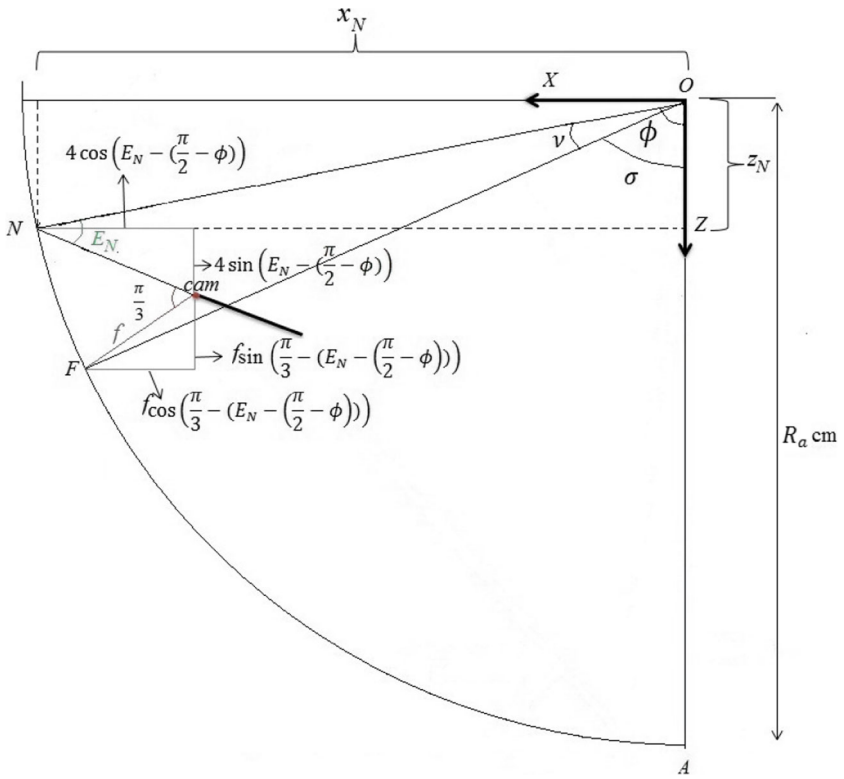

Fig. 15 The position of the capsule with respect to the greater curvature in *N-1*th movement step for $E_N < 0$

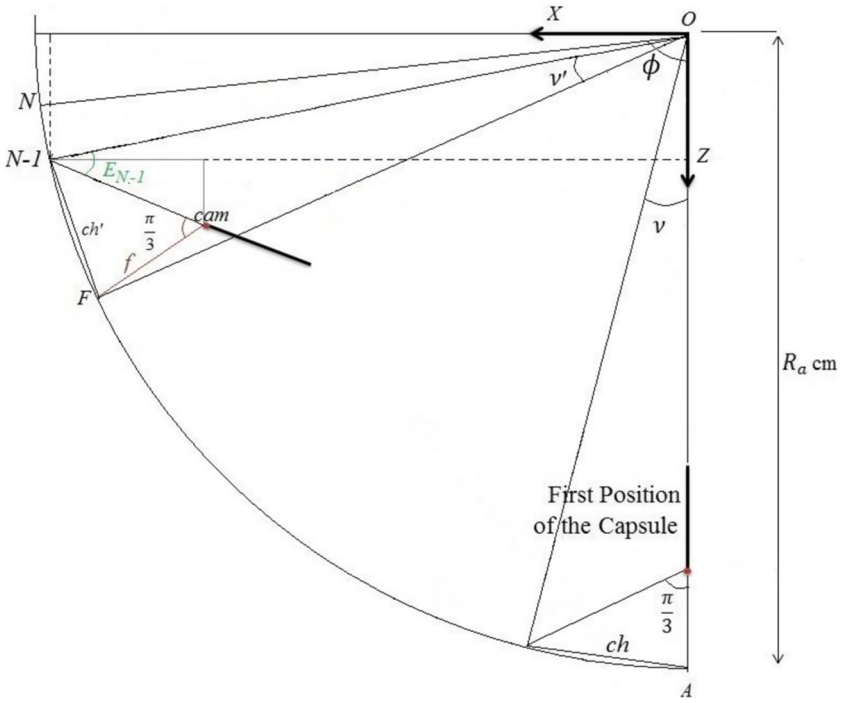

Fig. 16 The chords corresponding to the length of the images in XZ-plane

$$NF = R_a \nu \tag{20}$$

The Eqs. 19 to 20 are also obtained for $E_N < 0$ (Fig. 15):

$$\begin{aligned} x_{cam} &= R_a \sin(\phi) - 4\cos\left(E_N - \left(\frac{\pi}{2} - \phi\right)\right) \\ z_{cam} &= R_a \cos(\phi) + 4\sin\left(E_N - \left(\frac{\pi}{2} - \phi\right)\right) \end{aligned} \tag{21}$$

$$\begin{aligned} &\begin{cases} x_{cam} + f\cos\left(\frac{\pi}{3} - \left(E_N - \left(\frac{\pi}{2} - \phi\right)\right)\right) = R_a \sin(\sigma) \\ z_{cam} + f\sin\left(\frac{\pi}{3} - \left(E_N - \left(\frac{\pi}{2} - \phi\right)\right)\right) = R_a \cos(\sigma) \end{cases} \\ &\xrightarrow{Raise both sided to the power of 2} \left(x_{cam} + f\cos\left(\frac{\pi}{3} - (E_N\right.\right. \\ &\left.\left. - \left(\frac{\pi}{2} - \phi\right)\right)\right)^2 + \left(z_{cam} + f\sin\left(\frac{\pi}{3} - \left(E_N - \left(\frac{\pi}{2} - \phi\right)\right)\right)\right)^2 = R_a^2 \end{aligned} \tag{22}$$

$$\begin{aligned} x_F &= x_{cam} + f\cos\left(\frac{\pi}{2} - \phi + E_N + \frac{\pi}{3}\right) \\ z_F &= z_{cam} + f\sin\left(\frac{\pi}{2} - \phi + E_N + \frac{\pi}{3}\right) \end{aligned} \tag{23}$$

$$\begin{aligned} \nu &= \phi - \tan^{-1}\left(\left|\frac{x_F}{z_F}\right|\right) \\ NF &= R_a \nu \end{aligned} \tag{24}$$

e_d can be obtained with respect to Fig. 16 and by using the following steps.

1- The length of chord ch is calculated at the first position of the capsule where the capsule is perpendicular to the greater curvature. First, angle ν is calculated for $\phi = 0$, and then, ch is obtained according to Eq. 21. The length of ch is corresponding to half of the length of the acquired image by the camera.

$$ch = 2R_a \sin\left(\tfrac{\nu}{2}\right) \tag{25}$$

2- The length of chord ch' is calculated at the position of the capsule in $N-1$th movement step. First, angle ν' is calculated for $\phi = \phi - \frac{1+b\alpha}{R_a}$, and then, ch' is obtained according to Eq. 22. The length of ch' is corresponding to the length of the acquired image from the first column to the column which is corresponding to the position of the camera in $N-1$th step.

$$ch' = 2R_a \sin\left(\frac{\nu'}{2}\right) \tag{26}$$

3- $e_d = ch - ch'$.

Table 2 shows the impacts of the errors (that are calculated in Eqs. 18, 20 and 22) for the radii 6 and 20 cm and for three values of ϕ.

In order to decrease the impacts of the errors, the following method is proposed. Since this method can be used for stomach with unknown size, the proposed H-LC system is robust against the various sizes of the stomach.

At first, since the exact value of R_a is not known, the default value of 0.125 rad is selected for α. If the unfolded antrum can be seen in the half right side of the image in n_sth movement step, the value of R_a is estimated as follows:

1- The values of L (the length of the greater curvature) are calculated for different $n_s = N$ from 5 to 20 using

Table 2 The impacts of E_N

Radius of the Greater Curvature (R_a) (cm) / Angle ϕ (degree)	6	20
80	$\nu = 79.7°$	$\nu = 10.15°$
	$NF = 8.35cm$	$NF = 3.54cm$
	$e_d = 1.49cm$	$e_d = 2.04cm$
90	$\nu = 86.67°$	$\nu = 10°$
	$NF = 9.08cm$	$NF = 3.49cm$
	$e_d = 2.7cm$	$e_d = 2.1cm$
110	$\nu = 102.1°$	$\nu = 30°$
	$NF = 10.69cm$	$NF = 10.47cm$
	$e_d = 4.06cm$	$e_d = 1.52cm$

Eq. 23. These values are written in the second column of Table 3.

2- The new values are calculated for L according to the length of an arc in a circle relation ($L = R_a\phi$) and for R_a from 6 to 20 and for $\phi = 80°, 90° and 110°$.

3- The obtained values for L in step 2 are compared with the ones in step 1, the closest values are selected and the corresponding R_a's are specified.

4- The specified a's in step 3 are written in the third column of Table 3.

$$N = L/(1 + b\alpha) \Longrightarrow L = N(1 + b\alpha) \tag{27}$$

Table 3 The radii corresponding to different N

$n_s = N$	Length of the Greater Curvature (L) (CM)	Radius of the Greater Curvature (R_a) (cm)
7	8.1	6
8	9.8	7
9	11.4	8
10	13	9
11	14.6	10
12	16.3	11
13	17.9	12
14	19.5	13
15	21.1	14
16	22.8	15
17	24.4	16
18	26	17
19	27.6	18
20	2.3	19
21	30.9	20

The new value for α is calculated using the estimated R_a and (15). Then, the capsule is moved to the first position where was obtained in the secondary parking. Finally the rotation maneuver is applied by the new calculated α, which results in the minimum error.

2.5 Adjusting the Distance

Since the greater curvature is a curved-shape object, the depth of its points changes. Therefore, in order to have an image with proper scale, the depth of the capsule also should be changed so that the distance between the capsule and the greater curvature remains acceptable. To achieve this goal, the presented method in [28] is used.

3 Experimental Results and Discussion

3.1 Experimental Scenario

Before starting the endoscopy procedure, the clinician should proceed to in vitro calibration of the present capsule as it is explained in Section 2.1 (Fig. 17a) and form a table similar to Table 1. Then, the endoscopy procedure starts. The modus operandi of the proposed H-LC system for automatic endoscopy of the greater curvature by using the explained phases in sections 2.2 to 2.5 are as follows (Fig. 18).

1- The capsule is placed at the beginning of the greater curvature (either manually or automatically) in a proper distance (according to Section 2.1). Then, the reference and body coordinate systems are defined and the first movement step starts, $n_s = 1$ (Fig. 17b).

2- The image is acquired at the current position; the desired path is planned by using the method explained in Section 2.1. Points A and B are specified and ψ is calculated.

3- The capsule is rotated about the Z_C-axis by $\psi°$. Then, it is moved along the new Y_C-axis as Δy cm. Finally, it is transferred along the new X_C-axis as Δx cm. After these maneuvers, the position of the capsule with respect to the second reference coordinate system (${}^0_3\rho$) is calculated by the homogeneous transformation matrices as:

$${}^0_3\rho = {}^0_1H\,{}^1_2H\,{}^2_3H\,{}^3_3\rho,\ {}^3_3\rho = \begin{bmatrix} 0 \\ 0 \\ 0 \\ 1 \end{bmatrix} \tag{28}$$

$${}^0_1H = \begin{bmatrix} Rot_{Z_C,\psi} & 0 \\ 0 & 1 \end{bmatrix},\ Rot_{Z_C,\psi} = \begin{bmatrix} \cos(\psi) & -\sin?(\psi) & 0 \\ \sin(\psi) & \cos?(\psi) & 0 \\ 0 & 0 & 1 \end{bmatrix}$$

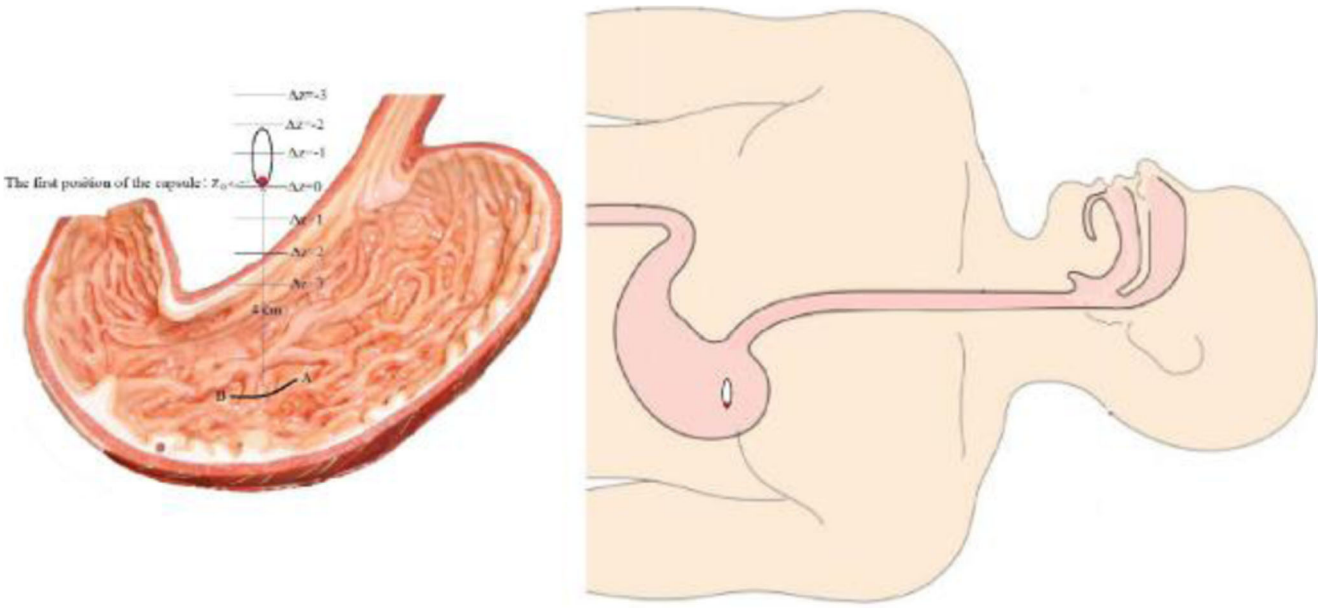

Fig. 17 **a** In vitro calibration of the present capsule **b** Parking the capsule at the beginning of the greater curvature

$$ {}^{1}_{2}H = \begin{bmatrix} I_{3\times3} & Trans_{X_C,\Delta x} \\ 0 & 1 \end{bmatrix}, Trans_{X_C,\Delta x} = \begin{bmatrix} \Delta x \\ 0 \\ 0 \end{bmatrix} $$

$$ {}^{2}_{3}H = \begin{bmatrix} I_{3\times3} & Trans_{Y_C,\Delta y} \\ 0 & 1 \end{bmatrix}, Trans_{Y_C,\Delta y} = \begin{bmatrix} 0 \\ \Delta y \\ 0 \end{bmatrix} $$

4- The capsule is rotated about the newY_C-axis by α degree. After applying this maneuver the position of the capsule with respect to the second reference coordinate system $({}^{0}_{4}\rho)$ is calculated as:

$$ {}^{0}_{4}\rho = {}^{0}_{1}H^{1}_{2}H^{2}_{3}H^{3}_{4}H^{4}_{4}\rho, {}^{4}_{4}\rho = \begin{bmatrix} 0 \\ 0 \\ 0 \\ 1 \end{bmatrix} \quad (29) $$

$$ {}^{3}_{4}H = \begin{bmatrix} Rot_{Y_C,\alpha} & 0 \\ 0 & 1 \end{bmatrix}, Rot_{Y_C,\alpha} = \begin{bmatrix} \cos(\alpha) & 0 & \sin(\alpha) \\ 0 & 1 & 0 \\ -\sin(\alpha) & 0 & \cos(\alpha) \end{bmatrix} $$

5- A new image is acquired and the scale factor between this new image and the acquired image in step 2 is derived. Then, the distance between the capsule and the surface of the greater curvature is adjusted. One movement step completes here. As a result, the final position of the capsule with respect to the second reference coordinate system after one movement step $({}^{0}_{n_s}\rho)$ is calculated as:

$$ {}^{0}_{n_s}\rho = {}^{0}_{1}H^{1}_{2}H^{2}_{3}H^{3}_{4}H^{4}_{5}H^{5}_{5}\rho, {}^{5}_{5}\rho = \begin{bmatrix} 0 \\ 0 \\ 0 \\ 1 \end{bmatrix} \quad (30) $$

$$ {}^{4}_{5}H = \begin{bmatrix} I_{3\times3} & Trans_{Z_C,\Delta z} \\ 0 & 1 \end{bmatrix}, Trans_{Z_C,\Delta z} = \begin{bmatrix} 0 \\ 0 \\ \Delta z \end{bmatrix} $$

6- n_s is increased by 1. Steps 2 to 6 are repeated until the unfolded antrum is seen. Finally, the value of n_s becomes equal to N.

3.2 Evaluation and Discussion

In order to evaluate the presented method for planning the desired path, it is applied on the 82 endoscopic frames with the size of 235 × 292 pixels acquired by the camera whose field of view is 140° and frame per second is 25. These images are captured from different parts of the greater curvatures of different people. They are acquired in various positions and orientations of the camera with different illumination values. The evaluation is done in MATLAB and using a Core™2Duo-2.80 GHz processor with 4GB RAM.

As it is mentioned in Section 1, in the literature related to steering and controlling of active capsule endoscopes

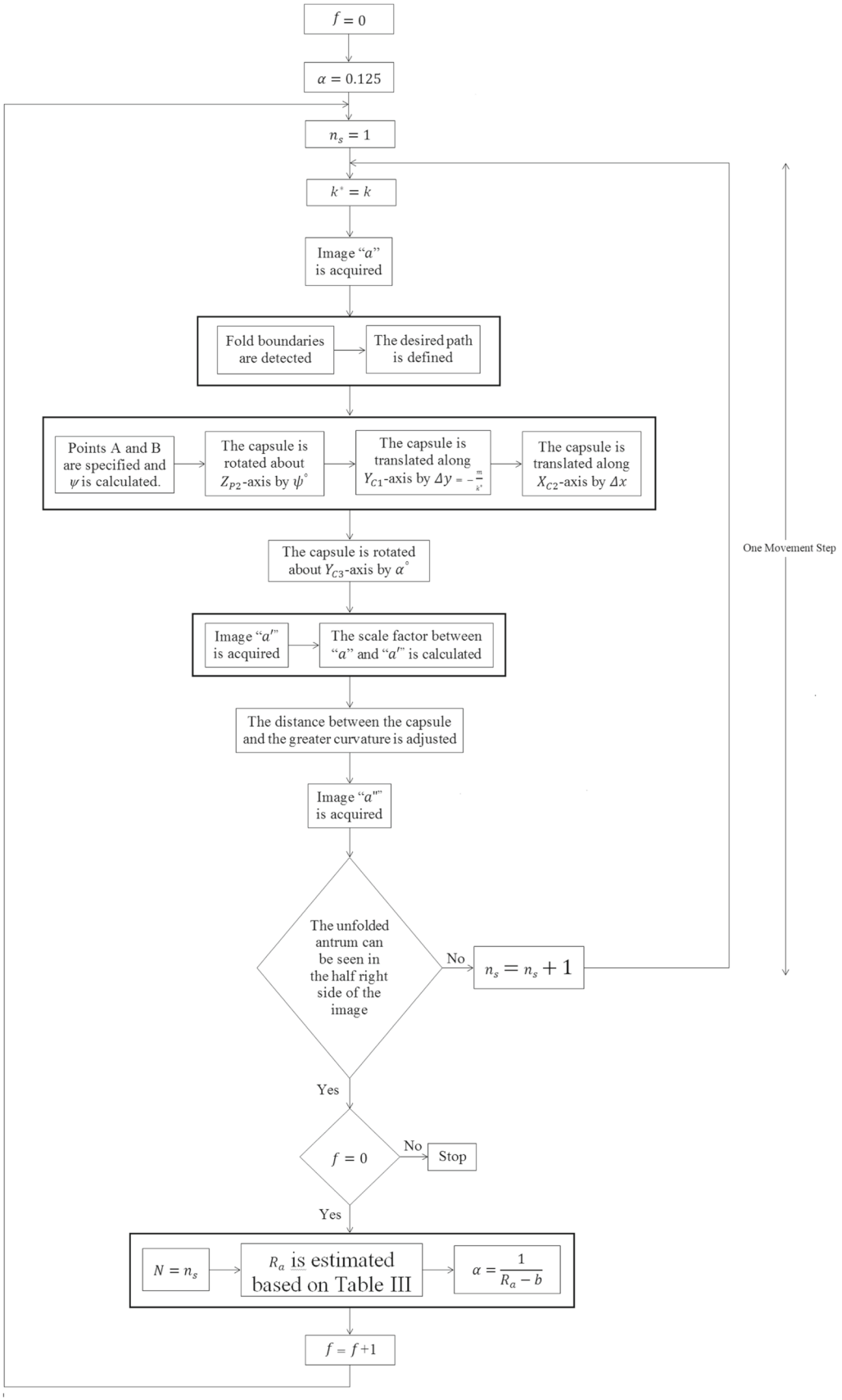

Fig. 18 The modus operandi of the proposed H-LC system

inside the stomach, the authors have developed methods in which an operator plays a high-level controller role and determines the new desired position and orientation of the capsule using the images acquired by the capsule. However, in our method, the desired positions and orientations of the capsule are determined automatically and without the need of the operator, which can lessen the problems made by the operator mistakes, e.g. missing some suspicious areas.

In [37] lumen detection is used for automatic control of the flexible endoscope tip orientation towards the direction of the lumen. However, this method is not useful for imaging of the stomach and can only be used for steering the tip to navigate the flexible endoscope through an endoluminal path. Since in our method, the main goal is automatic imaging of the stomach, the lumen detection is not a proper method due to the large open space in the stomach.

Use of the proposed approach improves the accuracy of the capsule endoscopy and makes the stomach examination easier and more convenient.

In order to grantee a real time autonomous examination, the required time for completing each movement step should be low enough so that the overall examination time remains in acceptable range (about 10-20 minutes due to remaining time of PEG in the stomach". The whole image processing procedures takes about 2 seconds for each movement step.

Figure 19a., displays the grayscale of the color image of the greater curvature based on the Section 2.2 for preparing the images to find the folds boundaries, and Fig. 19b and c. show the grayscale images after applying opening and closing operations.

Figure 20 depicts detecting the folds boundaries. Figure 20a, shows the image segmentation on the binary image, and in Fig. 20b the perimeter pixels, which demonstrate the boundaries, are specified.

The performance of the proposed method for detecting the folds boundaries is analyzed with respect to the ground truth images. The ground truth images are obtained by 3 experts who specify the boundaries in each image. To evaluate the results of the proposed method, the following parameters are used:

$$Sensitivity\,(SE) = \frac{TP}{TP + FN}$$
$$Specifity\,(SP) = \frac{TN}{TN + FP}$$
$$Accuracy\,(ACC) = \frac{TP + TN}{TP + TN + FP + FN}$$

in which, TP is true positive (the pixels of boundaries that are correctly identified), FP is false positive (the pixels that are incorrectly identified as boundaries), TN is true negative (the pixels that are correctly rejected), and FN is false negative (the pixels of boundaries that are incorrectly rejected). The averages of SE, SP and ACC for 82 images are obtained as 94%, 88% and 92%, respectively.

Figure 21 Shows the desired path in a binary image and in a grayscale endoscopic image according to the method presented in Section 2.2 for planning the desired path. It can be seen in this figure that by using the proposed method the holes have no effects in path planning.

Figure 22 shows the results of path planning method (explained in Section 2.2) for 6 sample frames. In this figure, the points A and B, which are described in Section 2.3, are also specified in each sample frame.

The values of ψ (radian) are calculated for each image of Fig. 22 according to the presented method in Section 2.3, as:

$$\psi = \begin{bmatrix} 0 & 0.0831 & -0.2450 \\ 0 & 0 & 0 \end{bmatrix}$$

As can be understood from Sections 2.2 and 2.3, the main purpose of the desired path planning is determining the line AB and following it by the capsule. To do this, the points A and B should be specified and the angle of line AB (ψ) should be calculated. For evaluating the performance of this

Fig. 19 An endoscopic image preprocessing: **a** the grayscale image, **b** the image after applying the opening operation, **c** the image after applying the closing operation

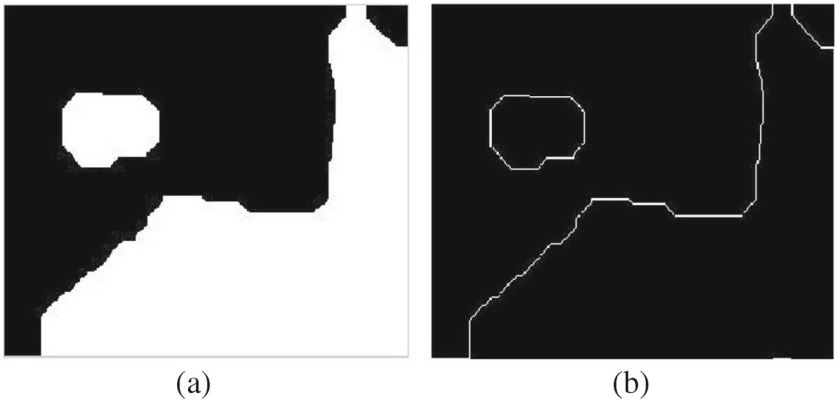

Fig. 20 Detection of the fold boundaries: **a** image segmentation on the binary image using active contours, **b** the perimeter pixels, which demonstrate the boundaries

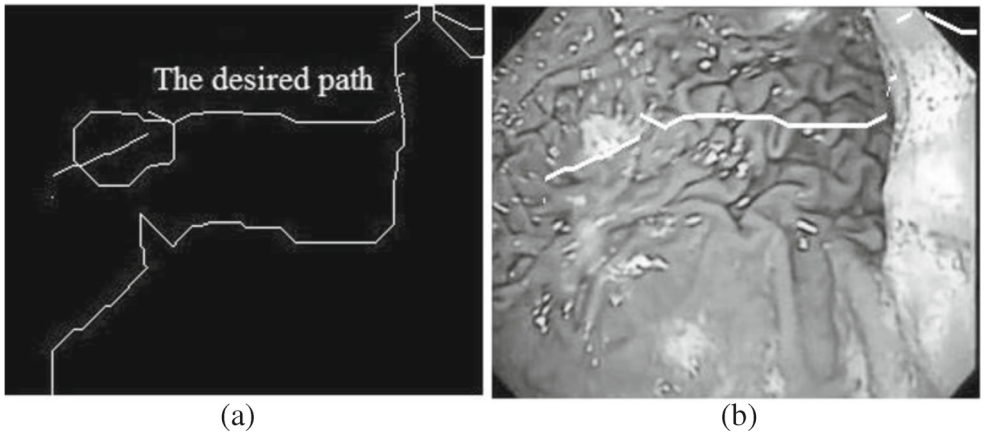

Fig. 21 Planning the desired path: **a** the desired path in a binary image, **b** the desired path in a grayscale endoscopic image

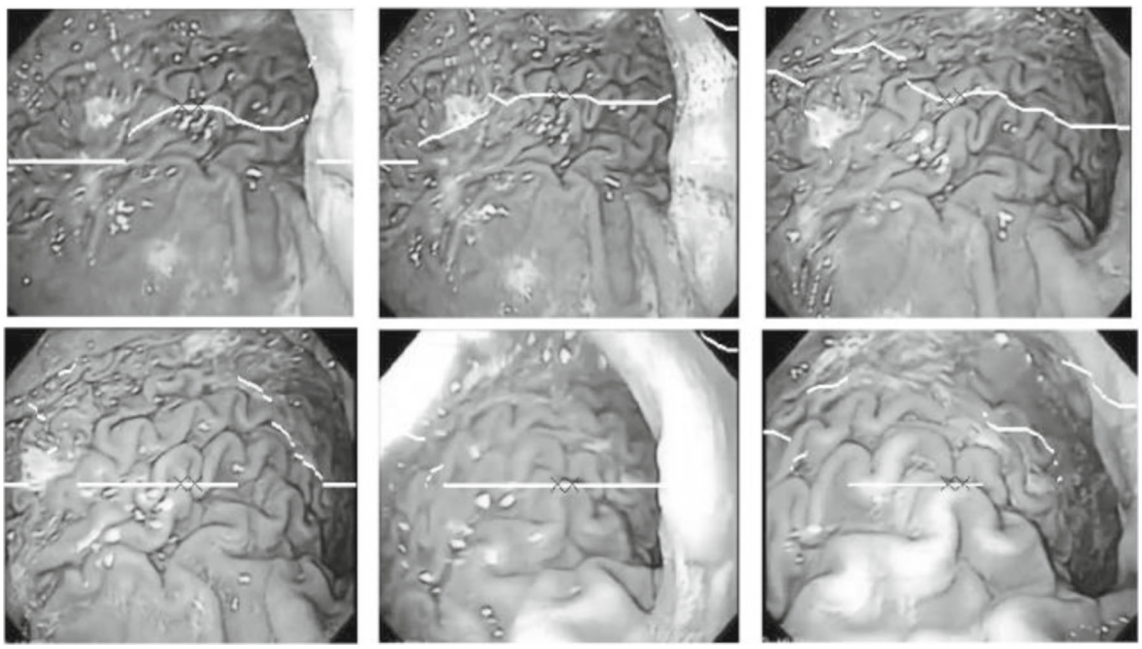

Fig. 22 The planned desired path in 6 sample frames

method, A, B and ψ are compared with A', $B' and \psi'$ that are specified in the images in which the folds boundaries are obtained by 3 experts. The accuracies are defined as the number of pixels between A and A' (ACA), the number of pixels between B and B' (ACB), and the difference between ψ and ψ' (ACL). The average of ACA is obtained as 3.66 pixels and the average of ACB is obtained as 3.72 pixels which are completely acceptable with respect to the number of images' pixels based on the experts opinion. The average of ACL is obtained as 0.005 rad which is ignorable.

For evaluating the calculated value of α using the method explained in Section 2.4, the impacts of non-perpendicularity, defined as mathematic parameters (ν, NF, e_d), are derived based on the default value of α (Table 2). According to Table 2, in the worst case, 3.49 cm of the length of the greater curvature is seen by the camera. Therefore, the value of CA_N for the worst case is equal to 3.49 cm. Although this value seems satisfactory, it is better to be increased. According to Table 2, the maximum e_d occurs for $R_a = 6$ cm and is 4.06 cm which is relatively large and it is better to be improved. By using the new value of α, theoretically the error in the last movement step (E_N) and consequently the impacts of non-perpendicularity should be equal to zero. But, because of the estimations in deriving the equations, they are not exactly equal to zero. However, they reach the possible minimum values. The following simulation is an example in which the real value of E_N is obtained.

For evaluating the introduced maneuvers for path following and maintaining the direction of the capsule perpendicular to the greater curvature (Sections 2.3 and 2.4), a simulation in MATLAB is used. Figure 23 shows different positions and orientations of the capsule after applying steps 3 and 4 (which are introduced in Section 3.1). In this simulation, the different parameters and different values of ψ in different movement steps are assumed as follows. Since all of these values are chosen completely arbitrary, the results are reliable.

$$R_a = 15, \phi = \frac{\pi}{2}\psi(radian) = \begin{bmatrix} 0.1651 \\ 0.1651 \\ 0.0831 \\ 0.1651 \\ 0.0831 \\ 0.0997 \\ 0 \\ 0 \\ -0.0611 \\ 0.0873 \\ -0.0698 \\ -0.1047 \\ 0.0401 \end{bmatrix}$$

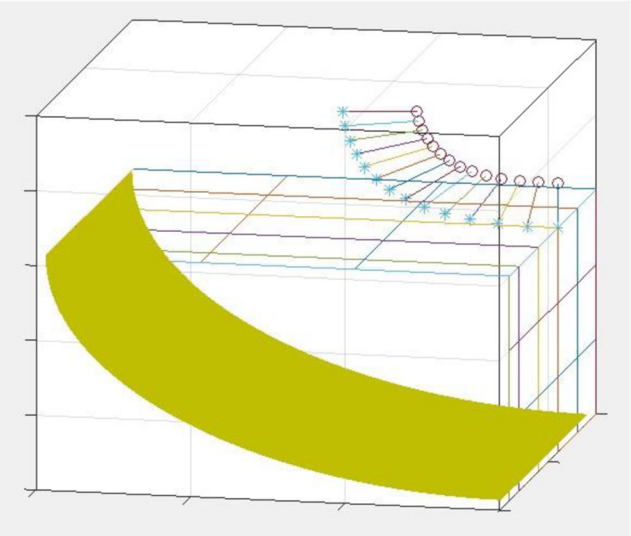

Fig. 23 Different positions and orientations of the capsule after applying the introduced maneuvers for following the desired path and maintaining the direction of the capsule toward the greater curvature. The stars are the symbols for the camera of the capsule

It is clear from Fig. 23 that by applying the maneuvers in steps 3 and 4, the capsule moves properly along the greater curvature while its direction is maintained toward the greater curvature. The error in the last movement step (E_N) in this example with calculated $\alpha \cong 0.07rad$, explained in Section 2.4, is equal to 1° while the error with the default value of $\alpha \cong 0.125rad$ is approximately equal to -48.5°.

For using the proposed H-LC system, the patient should lie on his left side so that the position of the stomach is as shown in Fig. 2. The stomach should be distended about 1 liter by deglutition of liquid solution of Polyetilenglycol (PEG). This liquid solution remains inside the stomach for about 10-20 min, which allows control of the capsule endoscope for examining the stomach during this time [10]. The H-LC system can be used for adult patients who have not had a stomach surgery because the general shape of the stomach usually changes after surgery.

4 Conclusion and Future Work

In this paper a novel real-time high-level control system for an active capsule endoscope is presented. This system provides autonomous control of an active capsule endoscope and automatic endoscopy of the biggest part of the stomach (the greater curvature). There are two main challenges which we try to solve in this paper:

1. Real-time planning the desired path and the maneuvers of an active capsule endoscope, equipped with only a monocular camera, while the exact shape and size of the

stomach is unknown, 2. Imaging of the greater curvature while the camera's optical axis of the capsule remains approximately perpendicular to the greater curvature during its movement.

A calibration method is proposed due to the needs of different phases of the proposed H-LC system. In the proposed H-LC system, first, the boundaries of the folds of the greater curvature are detected accurately and fast enough using image processing techniques. Then the desired path is planned using the path of the folds which is specified in the middle of the region where the folds are restricted to. For accurate following the desired path, three maneuvers are proposed. Two maneuvers are introduced so that the desired path is placed horizontally in the middle of the acquired images, and one maneuver is suggested for moving the capsule along the greater curvature.

In order to maintain the capsule direction perpendicular to the surface of the greater curvature, a rotation maneuver is proposed. For determining the suitable value of the rotation angle (α), geometric modeling and analysis are used. First the error of non-perpendicularity is defined as is explained in Section 2.4, and the value of the rotation angle corresponding to the minimum error is obtained based on the defined parameters. Then, the values of these parameters are specified based on previous works and some experimental measurements. As a result, an acceptable range is obtained for the rotation angle. Since the exact shape and size of the stomach is not known for different people, a method is proposed for determining the best value of α for each person. In this method, the default value is considered for α and the endoscopy procedure is done. When the examination of the greater curvature finishes, the best value of α is determined using the estimated radius of the greater curvature based on the number of movement steps. Then, the endoscopy procedure is repeated with the new value of α.

The last achievement of the proposed H-LC system is calculating the position vectors of the capsule with respect to the second reference coordinate system after applying each maneuver using homogenous matrices.

The proposed H-LC system ensures that the capsule's direction remains toward to the greater curvature during the endoscopy procedure while it doesn't have any contact with the walls of the stomach. As it is mentioned in Section 2 these features guarantee that the acquired images are suitable and useful, and the stomach is exposed to less damage. In the proposed H-LC system, the position of the capsule is quite clear; consequently, the positions of abnormalities and disorders can also be determined. Therefore, using the localization methods is not required when the H-LC system is used.

It should be noted that the presented H-LC system can be used for endoscopy of the lesser curvature by changing the position of the patient and applying some changes to the details of each phase.

We aim to design a suitable low-level control system for capsule endoscopy procedure. H-LC along with this system provides the automatic capsule endoscopy in which the human mistakes are minimized. Furthermore, we plan to enhance our method by providing a hybrid system in which the physician is able to choose between automatic and manual modes.

References

1. Slawinski, P.R., Obstein, K.L., Valdastri, P.: Emerging issues and future developments in capsule endoscopy. Tech. Gastrointest. Endosc. **17**(1), 40–46 (2015)
2. Ciuti, G., et al: Frontiers of robotic endoscopic capsules: a review. J. Micro-Bio Robot. **11**(1-4), 1–18 (2016)
3. Ciuti, G., Menciassi, A., Dario, P.: Capsule endoscopy: from current achievements to open challenges. IEEE Rev. Biomed. Eng. **4**, 59–72 (2011)
4. Singeap, A.M., Stanciu, C., Trifan, A.: Capsule endoscopy: the road ahead. World J. Gastroenterol. **22**(1), 369 (2016)
5. Menciassi, A., Ciuti, G., Cavallotti, C.: Future developments of video capsule endoscopy: hardware. In: Video Capsule Endoscopy: A Reference Guide and Atlas, pp. 543–556. Springer, New York (2015)
6. Zabulis, X., Argyros, A.A., Tsakiris, D.P.: Lumen detection for capsule endoscopy. In: IROS, pp. 3921–3926, Nice (2008)
7. Mura, M., et al: Vision-based haptic feedback for capsule endoscopy navigation: a proof of concept. J. Micro-Bio Robot. **11**(1–4), 35–45 (2016)
8. Rahman, I., Afzal, N.A., Patel, P.: The role of magnetic assisted capsule endoscopy (MACE) to aid visualisation in the upper GI tract. Comput. Biol. Med. **65**, 359–363 (2015)
9. Carta, R., et al: Wireless powering for a self-propelled and steerable endoscopic capsule for stomach inspection. Biosens. Bioelectron. **25**(4), 845–851 (2009)
10. De Falco, I.: An integrated system for wireless capsule endoscopy in a liquid-distended stomach. IEEE Trans. Biomed. Eng. **61**(3), 794–804 (2014)
11. Keller, J., et al: Inspection of the human stomach using remote-controlled capsule endoscopy: a feasibility study in healthy volunteers (with videos). Gastrointest. Endosc. **73**(1), 22–28 (2011)
12. Rahman, I., et al: Magnetic-assisted capsule endoscopy in the upper GI tract by using a novel navigation system (with video). Gastrointest. Endosc. **83**(5), 889–895 (2016)
13. Keller, H., et al. In: BioRob, pp. 859–865. Method for navigation and control of a magnetically guided capsule endoscope in the human stomach, Rome (2012)
14. Rey, J.F., et al: Blinded nonrandomized comparative study of gastric examination with a magnetically guided capsule endoscope and standard videoendoscope. Gastrointest. Endosc. **75**(2), 373–38 (2012)
15. Carpi, F., Kastelein, N., Talcott, M., Pappone, C.: Magnetically controllable gastrointestinal steering of video capsules. IEEE Trans. Biomed. Eng. **58**(8), 231–234 (2011)

16. Carpi, F., Pappone, C.: Magnetic maneuvering of endoscopic capsules by means of a robotic navigation system. IEEE Trans. Biomed. Eng. **56**(5), 1482–1490 (2009)
17. Mahoney, A.W., Abbott, J.J.: Five-degree-of-freedom manipulation of an untethered magnetic device in fluid using a single permanent magnet with application in stomach capsule endoscopy. Int. J. Robot. Res. **35**(1–3), 129–147 (2016)
18. Abu-Khalil, Y., et al.: Vision and inertial-based image mapping for capsule endoscopy. In: ICTRC, pp. 84–87, Abu Dhabi (2015)
19. Sehyuk, Y., Sitti, M.: 3-D localization method for a magnetically actuated soft capsule endoscope and its applications. IEEE Trans.Robot. **29**(5), 1139–1151 (2013)
20. Azizian, M., Khoshnam, M., Najmaei, N., Patel, R.V.: Visual servoing in medical robotics: a survey. part i: endoscopic and direct vision imaging techniques and applications. Int. J. Med. Robot. **10**(3), 263–274 (2014)
21. Wang, Y., et al: Vision-based road detection by monte carlo method. Inf. Technol. J. **9**(3), 481–487 (2010)
22. Rasmussen, C., Lu, Y., Kocamaz. M.: Appearance contrast for fast, robust trail-following. In: IROS, pp. 3505–3512, St. Louis (2009)
23. Kong, H., Audibert, J.Y., Ponce, J.: General road detection from a single image. IEEE Trans. Image Process. **19**(8), 2211–2220 (2010)
24. Blas, M.R., et al.: Fast color/texture segmentation for outdoor robots. In: Intelligent Robots and Systems. IROS, pp. 4078–4085, Nice (2008)
25. Ulrich, I., Nourbakhsh, I.: Appearance-based obstacle detection with monocular color vision. In: AAAI/IAAI. Austin, pp. 866–871 (2000)
26. Santosh, D., Achar, S., Jawahar, C.V.: Autonomous image-based exploration for mobile robot navigation. In: ICRA, pp. 2717–2722, California (2008)
27. De Cristóforis, P., et al: Real-time monocular image-based path detection. J. Real-Time Image Proc. **11**(2), 335–348 (2016)
28. Aghanori, M., Ghaffari, A., Dadashi, N. In: BHI, pp. 13–16, Orlando (2017)
29. Snell, R.S.: Clinical anatomy, 7th edn. Lippincott Williams & Wilkins (2004)
30. Lam, M., Mintchev, M.: Diamagnetically stabilized levitation control of an intraluminal magnetic capsule. Physiol. Meas. **30**(8), 763 (2009)
31. Lee, S.H., et al.: Technical skills and training of upper gastrointestinal endoscopy for new beginners. World J. Gastroenterol.: WJG **21**(3), 759–785 (2015)
32. Gonzalez, R.C., Woods, R.E. Digital image processing, 2nd edn. Prentice-Hall, Upper Saddle River (2002)
33. Chan, T.F., Vese, L.A.: Active contours without edges. IEEE Trans. Image Process **10**(2), 266–277 (2001)
34. National Research Council: Risk assessment of radon in drinking water. National Academy of Sciences, Washington (1999)
35. Gray, H., Standring, S.: Gray's anatomy: the anatomical basis of clinical practice, 40th edn. In: Churchill-Livingstone, Spain (2008)
36. Liao, D., et al: Analysis of surface geometry of the human stomach using real-time 3-D ultrasonography in vivo. Neurogastroenterol. Motil. **16**(3), 315–324 (2004)
37. Reilink, R., Stramigioli, S., Misra, S.: Image-based flexible endoscope steering. In: IROS, pp. 2339–2344, Taipei (2010)

Mehrnaz Aghanouri was born in Isfahan, Iran, in 1989. She received her B.S. degree in Mechanical Engineering from the Isfahan University of Technology, Isfahan, Iran, in 2012 and her M.S. degree in Mechatronics Engineering from the K. N. Toosi University of Technology, Tehran, Iran, in 2017.

She was a Teacher Assistant with the Mechanical Engineering Department, K. N. Toosi University of Technology, in 2016. She is currently a senior researcher at Medical Image and Signal Processing research Center and a PhD student of Medical Robotics at Tehran University of Medical Sciences. Her research interests include medical robotics, mechatronics, control, image and video Processing, and computer vision.

Ali Ghaffari was born in Neishabour, Iran, in 1947. He received the B.S. degree in Mechanical Engineering from Sharif University of Technology, Tehran, Iran, in 1971, the M.S. degree in Mechanical Engineering from Georgia Institute of Technology, Atlanta, in 1975, and the Ph.D. degree in Mechanical Engineering from the University of California, Berkeley, in 1978.

He is currently a Professor with the Department of Mechanical Engineering, K. N. Toosi University of Technology. He is also the Head of the Cardio Vascular Research Center, Department of Mechanical Engineering. He is the Editor of the International Journal of Robotics and has collaborated with different firms on applied projects. His main research interests include linear and nonlinear modeling and control systems, intelligent control, fuzzy logic, robotics, and bioengineering.

Nasim Dadashi Serej was born in Tabriz, Iran, in 1980. She received the B.S. degree in Bio-Electrical engineering from Sahand University of Technology, Tabriz, Iran, the M.S. degree in Bio-Medical engineering from Isfahan University of Medical Sciences, and the Ph.D. degree in Bio-Medical engineering from the Tehran University of Medical Sciences.

She is currently a member of School of Advanced Technologies in Medicine, a senior researcher at Medical Image and Signal Processing research Center and a member of editorial office of Journal of Medial Signals and Sensors. Her main research areas are image and video Processing, 3D computer vision with primary emphasis on 4D reconstruction, pose estimation, and motion estimation.